AGU PUBLICATIONS

JGR

Journal of Geophysical Research: Oceans

RESEARCH ARTICLE

10.1002/2017JC013340

Satellite Altimetry and Current-Meter Velocities in the Malvinas Current at 41°S: Comparisons and Modes of Variations

Ramiro Ferrari[1], Camila Artana[2], Martin Saraceno[3], Alberto R. Piola[4], and Christine Provost[2]

[1]CIMA/CONICET-UBA and UMI IFAECI-3351, Buenos Aires, Argentina, [2]Laboratoire LOCEAN-IPSL, Sorbonne Universités (UPMC, Univ. Paris 6)-CNRS-IRD-MNHN, Paris, France, [3]CIMA/CONICET-UBA, DCAO/FCEN/UBA and UMI IFAECI-3351, Buenos Aires, Argentina, [4]Departamento de Oceanografía, Servicio de Hidrografía Naval, DCAO/FCEN/UBA and UMI IFAECI-3351, CONICET, Buenos Aires, Argentina

Abstract Three year long current-meter arrays were deployed in the Malvinas Current at 41°S below a satellite altimeter track at about 10 years intervals. Surface geostrophic velocities (SGV) derived from satellite altimetric data are compared with the in situ velocities at the upper current meter (∼300 m). Multisatellite gridded SGV compare better with in situ observations than along-track SGV. In spite of the proximity of the moorings to the complex Brazil-Malvinas Confluence (BMC) region, satellite SGV are significantly correlated with the 20 day low-passed in situ velocities (0.85 for along-isobaths velocities, 0.8 for cross-isobaths velocities). The recent in situ measurement period (2014–2015) stands out in the altimetry record with a long-lasting (4 months) high level of eddy kinetic energy at the mooring site and a southernmost location of the Subantarctic Front (SAF). The first two modes of variations of sea level anomaly (SLA) over the BMC remarkably match the first two modes of the low-passed in situ velocities. The first mode is associated with a latitudinal migration of the SAF, and the second with a longitudinal displacement of the Brazil Current overshoot. The two modes dominate the 24 year long record of SLA in the BMC, with energy peaks at the annual and semiannual periods for the first mode and at 3–5 months for the second mode. The SLA over the Southwest Atlantic was regressed onto the two confluence modes of SLA variations and showed remarkable standing wave train like structures in the Argentine Basin.

Key Points:
- Satellite-derived surface velocities and 20 day low-passed in situ velocities at 300 m from three data sets are highly correlated (>0.8)
- In the 24 year long altimetric record, the 2014–2015 mooring period stands out with a southernmost location for the Subantarctic Front
- Two modes dominate velocity variations: meridional motions of the Subantarctic Front and zonal motions of the Brazil Current overshoot

Correspondence to:
R. Ferrari,
ramiro.ferrari@cima.fcen.uba.ar

Citation:
Ferrari, R., Artana, C., Saraceno, M., Piola, A. R., & Provost, C. (2017). Satellite altimetry and current-meter velocities in the Malvinas Current at 41°S: Comparisons and modes of variations. *Journal of Geophysical Research: Oceans*, *122*. https://doi.org/10.1002/2017JC013340

Received 7 AUG 2017
Accepted 3 NOV 2017
Accepted article online 30 NOV 2017

1. Introduction

The Malvinas Current (MC) is a narrow branch of the Antarctic Circumpolar Current (ACC) that flows northward along the continental slope of Argentina until it meets the southward flowing Brazil Current (BC) at approximately 39°S (Figures 1a and 1b). After the collision, both currents separate from the slope and turn offshore. The MC retroflects cyclonically southward, whereas the BC separates into two branches, one branch recirculating northward, while the other branch flows southward and returns to the northeast at about 45°S (Peterson & Stramma, 1991). The latter branch is referred to as the overshoot of the Brazil Current. The confluence of the Brazil and Malvinas Currents creates a region of intense mesoscale variability, one of the most energetic regions of the world ocean (e.g., Chelton et al., 2007).

Satellite altimetry has provided new insights on the dynamics of the Southwest Atlantic either by itself or in conjunction with the rather scarce in situ data in the area: on the extraordinary eddy field (e.g., Fu, 2006; Mason et al., 2017; Provost & Le Traon, 1993; Saraceno & Provost, 2012), on the dynamics of the Zapiola anticyclone that occupies the center of the Argentine Basin (e.g., Fu, 2007; Fu et al., 2001; Saraceno et al., 2009), on the dynamics of the Malvinas Current (e.g., Artana et al., 2016; Piola et al., 2013; Spadone & Provost, 2009; Vivier & Provost, 1999b).

The first current-meter data on the MC were gathered, as part of the World Ocean Circulation Experiment (WOCE) program, at 41°S along TOPEX-POSEIDON track 26 across the continental slope near the Brazil/Malvinas Confluence from December 1993 to June 1995 (Vivier & Provost, 1999a) (Figure 1, green dots). These measurements showed that the flow of the MC had mainly an equivalent barotropic vertical structure and that the volume transport of the MC could be monitored with accuracy using altimetric data (Vivier & Provost, 1999b). A 5 year long volume transport time series (1992–1997) was produced and its intraseasonal variability analyzed (Vivier et al., 2001). Six years later, as a contribution to the Climate Variability and

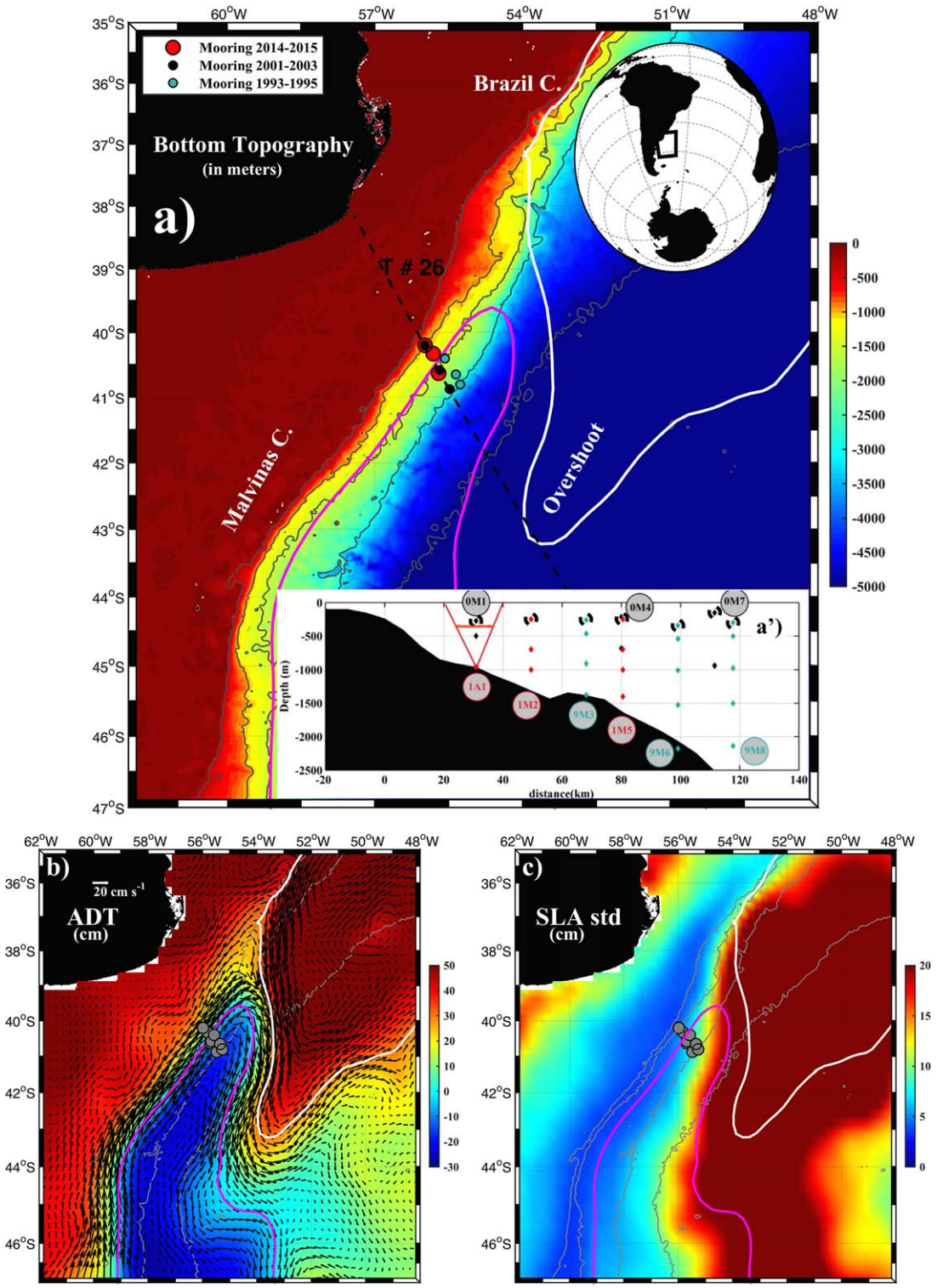

Figure 1. (a) Bottom topography of the Southwestern Atlantic (in meters) from Smith and Sandwell (1994) and location of the current-meter moorings (2014–2015, 2001–2003, and 1993–1995 in red, black, and green, respectively) deployed along the Jason satellite altimeter track #26. The 6,000, 5,000, 3,000, 1,000, and 300 m isobaths are represented with solid light grey contours. Spatial distribution of the current meters is shown in the lower right plot. The 0 km is referenced to the 300 m isobath. (b) Mean Absolute Dynamic Topography (ADT) with surface geostrophic velocities over 24 year of altimetric data (1993–2016). The mean location of the Subantarctic Front (SAF) (magenta line) and Brazil Current Front (BCF) (white line) correspond to ADT values of −5 and +30 cm, respectively. These values were defined as the location of the maximum gradients in the mean ADT (same procedure as in Barré et al. (2011)). (c) Standard deviation of the Sea Level Anomalies (SLA) over 24 years of altimetric data time series (1993–2016). Mooring locations are indicated in grey.

Prediction program (CLIVAR), an array of three current-meter moorings was deployed from December 2001 to February 2003 at the same location as the WOCE moorings. The CLIVAR moorings provided new information on the core of the MC over the 1,000 m isobaths where a mooring had been previously lost (Spadone & Provost, 2009) (Figure 1, black dots). A 14 year long time series of MC volume transport was then computed using both in situ data sets and satellite altimetry. Recently, as part of the Southwestern Atlantic Currents from Satellite Altimetry and in situ data (CASSIS-MALVINAS) project, a new velocity data set (2014–2015) was retrieved at the same location across the slope from three moorings including an ADCP deployed over the 1,000 m isobath (http://www.cima.fcen.uba.ar/malvinascurrent/en/) (Figure 1, red dots). A first objective of this work is to compare satellite altimetry products with in situ observations. This analysis is particularly relevant because the moorings are located next to the Brazil-Malvinas Confluence (Figure 1b), a region characterized by high eddy kinetic energy and short spatial and temporal scales of velocity variations (e.g., Barré et al., 2006). Another objective of this work is to put the 3 year long in situ measurements in a wider regional and temporal perspective by jointly analyzing them with the continuous 24-long satellite altimetry observations.

The paper is organized as follows. The data are presented in section 2. Precise comparisons between in situ velocities and surface velocities derived from altimetric data follow in section 3. The skill of the satellite altimetry products in this complicated boundary current region having been assessed, altimetric data are used, in section 4, to put the in situ point measurements into a larger temporal and spatial contexts. In section 5, it is shown that the principal modes of variations of sea level anomalies from satellite altimetry in the Confluence region match remarkably well the dominant modes of the in situ velocity variations and enable to interpret them. Then, we examine the modes of sea level anomaly (SLA) in the Confluence region using the 24 years of satellite data and seek statistical relationships with SLA variations in the whole Southwest Atlantic. Finally, results are summarized and perspectives are discussed in section 6.

2. Data

2.1. Mooring Data Over the Continental Slope of Argentina

We use the in situ velocities acquired over the western slope of the Argentine Basin slope, focusing on the longest time series of the upper-level velocity records deployed during 1991–1995 (9M3 at 240 m, 9M6 at 340 m, and 9M8 at 300 m), 2001–2003 (0M1 at 270 m, 0M4 at 215 m, and 0M7 at 150 m), and 2014–2015 periods (ADCP (1A1) at 328 m, moorings 1M2 at 377 m, and 1M5 at 520 m) lined up near the Brazil-Malvinas Confluence at 41°S along the historical TOPEX-Poseidon and Jason altimetric satellite track 26 (Figure 1 and Table 1). The records of raw velocity data were low-pass filtered (Loess filter) with a cutoff period of 48 h in order to remove inertial and tidal variance in the first instance and then low-pass filtered with different cutoff periods (5, 7, 10, 15, 20, and 30 days) and resampled at a daily rate for the purpose of comparing the surface geostrophic velocities computed from different altimetric products with the in situ velocities obtained at the upper current meter (Provost et al., 2017a, 2017b; Saraceno et al., 2017).

Table 1
Location and Length of the Current-Meter Records

Moorings	Latitude (°S)	Longitude (°W)	Depth (m)	Upper-level current-meter depth (m)	Days
2014–2015 current meter					
1A1	40.20	55.98	1,030	328	332
1M2	40.32	55.78	1,319	377	332
1M5	40.63	55.67	1,945	520	332
2001–2003 current meter					
0M1	40.20	55.98	1,010	270	416
0M4	40.58	55.68	1,510	215	426
0M7	40.88	55.48	2,536	150	179
1993–1995 current meter					
9M3	40.41	55.98	1,507	240	386
9M6	40.65	55.35	2,200	340	539
9M8	40.81	55.27	3,040	300	546

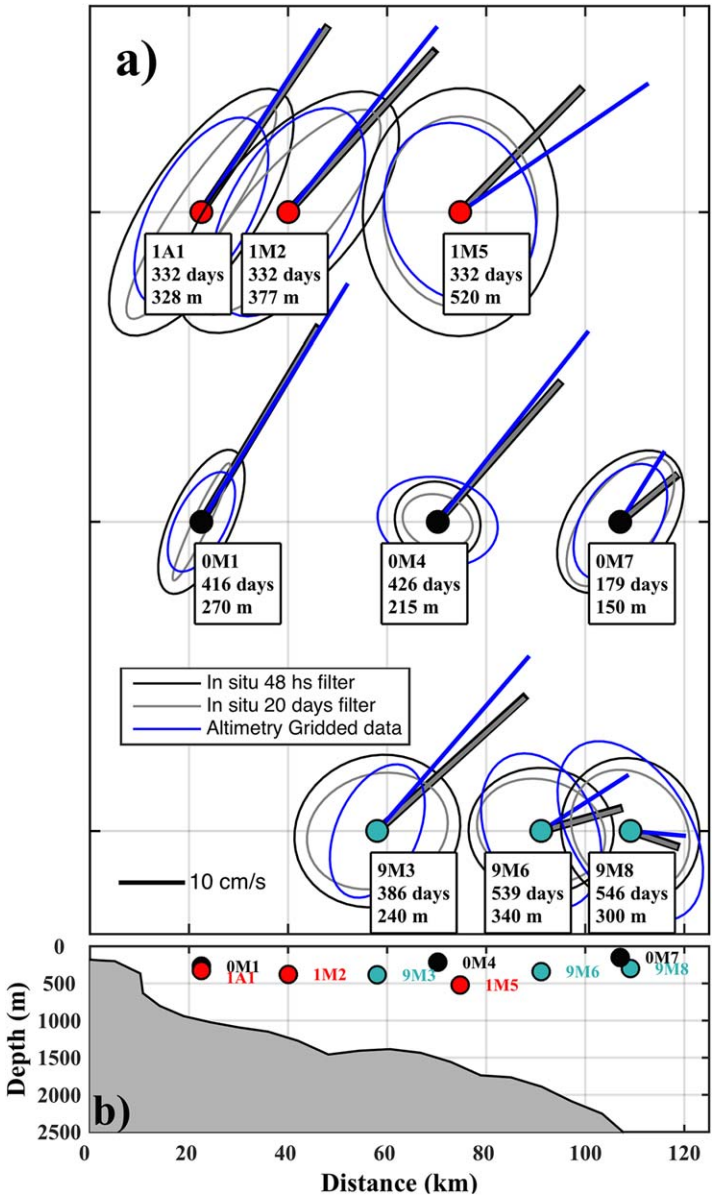

Figure 2. (a) Mean and variance ellipses of the satellite-altimeter-derived surface velocities and the in situ velocities from 2014 to 2015 (top in red), 2001 to 2003 (middle in black), and 1993 to 1995 (bottom in green). Means and ellipses of the in situ velocities with 2 and 20 days low-pass-filtered are plotted in black and grey, respectively. The surface velocities were computed from maps of absolute dynamic topography with a 1 day sampling from Altimeter multisatellite gridded products (MGP, in blue). (b) Location of the upper current meters along the slope is indicated in the lower plot (same color code for deployment years). The 0 km is referenced to the 300 m isobath.

2.2. Satellite Data

We used two types of altimetric products produced as part of the Copernicus Marine Environment monitoring service (CMEMS) (http://marine.copernicus.eu/): DUACS delayed time multisatellite gridded products (MGP) and along-track Jason data (ATJD) (Pujol et al., 2016). The MGP used here include absolute dynamic topography (ADT), surface geostrophic velocities (SGV), and sea level anomalies (SLA) with daily sampling and a spacing of $^1/_4$ degree in a Cartesian regular grid (8,766 maps from January 1993 to December 2016). The along-track product consists of ADT available since October 1992 with a temporal sampling of 10 days and a spatial sampling of 14 km low-pass filtered with a cutoff wavelength of 65 km. A 24 year long time series of surface geostrophic velocities were derived from the along-track data. For comparisons, surface geostrophic velocities computed from altimetric products were linearly interpolated at the mooring positions.

3. Satellite-Derived Surface Geostrophic Velocities at the Mooring Sites

3.1. Mean Flow and Variability

Mean surface velocities derived from altimetry (MGP) and mean in situ velocities at the mooring upper level have comparable directions and amplitudes (difference less than 15 degrees and 7 cm s^{-1}, respectively) in the MC on the western slope of the Argentine Basin (Figure 2 and Table 2). The comparable direction is consistent with a barotropic equivalent flow along the slope (Vivier & Provost, 1999a).

Though larger variance ellipses might be expected at the surface than at depth, this is seldom the case as the altimetry sampling cannot capture all the variability (e.g., 1A1, 1M2, 0M1). In general, surface velocities derived from altimetry provide a reasonable estimate of the in situ velocity variance when the in situ velocity is smoothed with a 20 day low-pass filter (Figure 2). This is consistent with the altimeter data sampling given by the Jason series (i.e., 10 day sampling) and the correlation scales used in the MGP processing (nearly 15 days in the area) (Pujol et al., 2016). On the steep slope, where the variance ellipses are stretched parallel to the isobaths (0M1, 1A1, 1M2), the large differences (>4 cm s^{-1}) in the minor axes between the 2 and 20 day low-pass-filtered velocities are due to the filtering out of the high frequencies in the across-track velocity component.

In situ data variance ellipses vary by a factor 2 from one data set to the other: they are largest during the last deployment and smallest during the second one. Altimetry-derived ellipses vary accordingly, and altimetry is used to put the different mooring periods in a wider regional and temporal perspective in section 4.

3.2. Comparison Between In Situ and Satellite-Derived Velocity Time Series

Upper-level in situ and altimetric velocities were rotated to compute the along/across-track component, parallel/perpendicular to the Jason track #26. For comparison, in situ data were low-pass-filtered with different cutoff periods ranging from 2 to 30 days (section 2.1). The comparison is shown for the three 2014–2015 moorings (Figure 3, 1A1, 1M2, and 1M5). In situ cross track velocities exhibit a large range of values from −30 to +70 cm s^{-1} (Figures 3a–3c) whereas along-track velocities show smaller amplitudes (−30 to +30 cm s^{-1}) with rather high frequency variations (Figures 3d–3f). The spatial set up (Figure 3g) with the three moorings within a 60 km distance (red dot and diamonds), the satellite track #26 (thick black line),

Table 2
Statistics of Altimetrically Derived Surface Geostrophic Velocities and Upper Current-Meter Measurements (2 and 20 Day Low-Pass-Filtered and Daily Resampled) From the 2014 to 2015, 2001 to 2003, and 1993 to 1995 Mooring Arrays

	V (cm s^{-1})		Ang (V) (deg)		Major axis (cm s^{-1})		Minor axis (cm s^{-1})	
Current meters	In situ	MGP	In situ	MGP	In situ 2 d filter (20 d filter)	MGP	In situ 2 d filter (20 d filter)	MGP
2014–2015								
1A1 328 m	35.82	35.02	34.19	33.08	23.28 (20.65)	16.99	8.89 (4.25)	7.94
1M2 377 m	34.91	38.16	42.18	38.72	24.05 (21.27)	18.64	11.20 (6.83)	9.53
1M5 520 m	27.59	34.51	44.45	55.59	20.06 (15.51)	14.75	15.73 (12.46)	11.91
2001–2003								
0M1 270 m	36.32	43.11	30.91	31.55	12.64 (10.49)	8.82	4.98 (1.29)	4.05
0M4 215 m	29.59	36.57	41.27	38.35	7.04 (5.76)	9.79	6.37 (4.34)	7.15
0M7 150 m	11.40	13.14	50.53	36.23	13.15 (12.24)	10.37	8.03 (5.85)	6.11
1993–1995								
9M3 240 m	31.89	37.11	47.63	40.91	13.62 (11.59)	11.46	12.09 (9.17)	6.60
9M6 340 m	13.01	16.45	74.52	59.73	11.72 (10.53)	13.14	10.22 (8.26)	8.91
9M8 300 m	7.67	8.67	108.28	94.99	11.96 (10.59)	16.03	11.02 (8.81)	9.52

Note. V is the modulus of the time-averaged velocity and ang (V) is the angle of the mean velocity relative to the north (positive is clockwise). Major axis and minor axis are the lengths of the standard deviation ellipse axes.

and the Cartesian regular grid (colored) shows that the comparison is challenging as the differences between the in situ velocities are considerable (e.g., Figures 3a and 3c). Correlations between across-track (along-track) component of the altimetric surface and 2 day low-pass-filtered in situ velocities range from 0.80 (0.50) to 0.68 (0.65) for the 2014–2015 upper-level data (Table 3). The corresponding vector correlations range from 0.7 to 0.9 and root mean square differences (rmsd) from 11.3 to 14.2 cm s^{-1} (Table 3). The agreement between the in situ and satellite-derived velocities increases with in situ data smoothing scale and the rmsd decreases by more than 3 cm s^{-1} when a 20 day low-pass filtered is applied to the in situ data (Table 3).

Altimetry-derived and in situ velocities comparisons for the 2001–2003 and 1993–1995 periods yield similar results. In general, correlations between the in situ and altimetric velocities monotonically increase while the rmsd monotonically decrease up to the 20 days cutoff period (Tables 3 and 4). The mean rmsd between satellite-altimeter-derived surface velocities and 20 day low-pass-filtered upper current-meter velocities from all moorings is 7 cm s^{-1} (Table 3). The correlations between the across-track (i.e., nearly along isobaths) velocity component are larger ($\sim$0.85) than between the along-track (nearly cross isobaths) velocity components ($\sim$0.8) (Table 3).

Mooring data, acquired along Jason satellite ground-track #26, also provide the opportunity to compare across-track velocities derived from along-track satellite product (yellow stars and line in Figure 3). Table 4 shows that the MGP compare better than along-track SLA derived velocities, with smaller rmsd than the Jason along-track data. The reduction in rmsd from along-track to MGP data varies from 6% to 68% (Table 4). Hence, the improved time resolution provided by the multisatellite products makes these preferable to the single satellite along-track data for examining the geostrophic circulation, and in the following, we use the MGP products.

4. Interpretation of Current-Meter Data in Light of Altimetry

4.1. The Three Mooring Periods Within the 24 Years of Altimetry

As noticed in section 3.1, velocity variance ellipses vary between deployment periods to other by a factor two, being largest during the most recent deployment (2014–2015). The altimetry-derived eddy kinetic energy (EKE) time series computed over a box centered on the mooring array (Figure 4a) shows that the last mooring deployment period (December 2014 to November 2015) is characterized by an exceptional long-lasting episode of high EKE values, exceeding 500 cm^2 s^{-2} during 4 months from 1 May to 1 September 2015 (Figure 4b). No similar episodes are observed in the altimetric record since January 1993. Some aperiodic EKE peaks are observed in the time series but they do not last more than a month (Figure 4b).

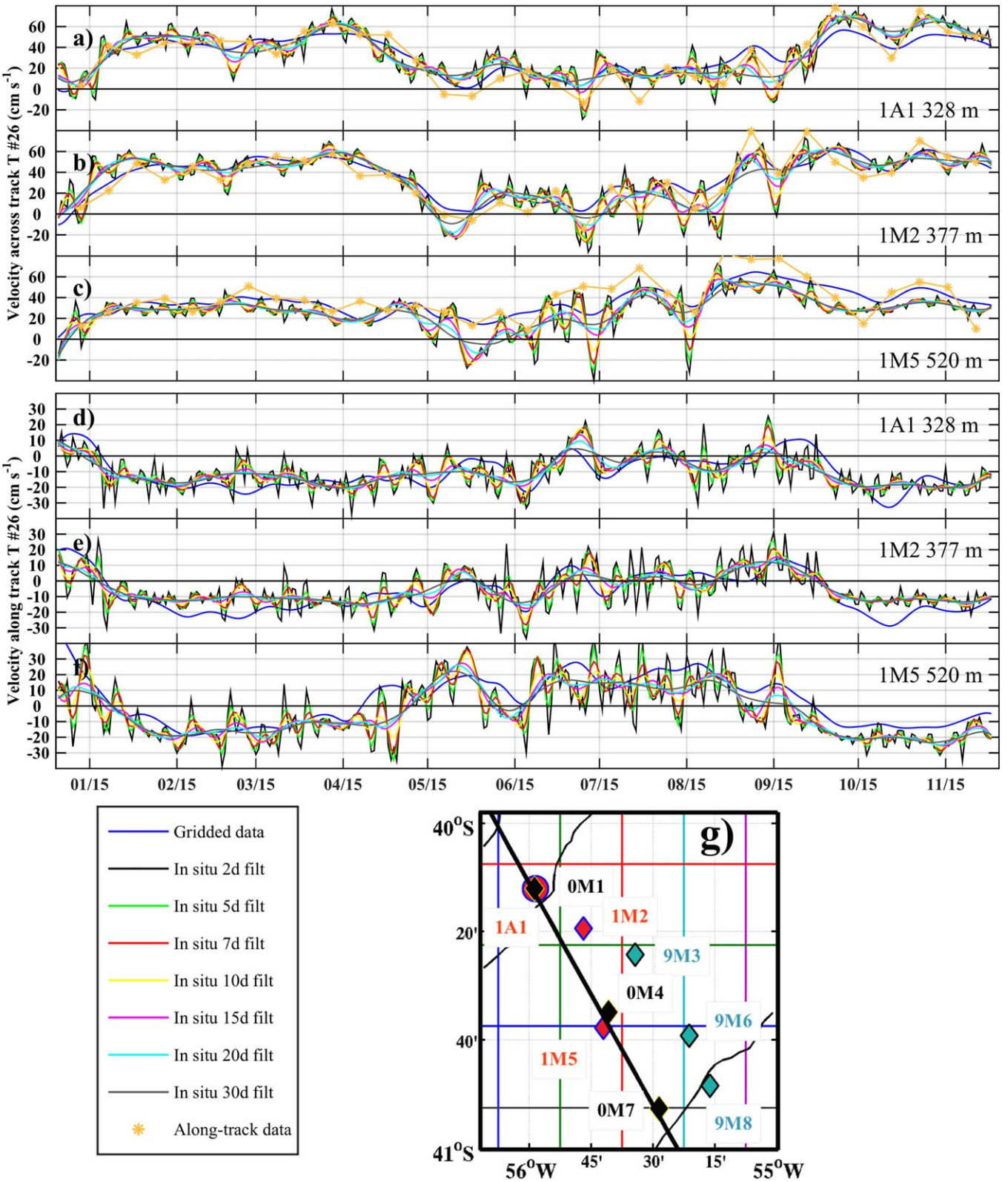

Figure 3. (a–c) Across and (d–f) along Jason track #26 components of the surface velocities derived from altimetry and from the upper-level in situ velocities at (a and d) 1A1, (b and e) 1M2, and (c and f) 1M5. Surface velocities were computed from Multisatellite gridded products (MGP, shown in blue) with daily sampling. In situ velocities shown in black, green, red, yellow magenta, light blue, and grey were computed with a 2, 5, 7, 10, 15, 20, and 30 days low-pass-filtered and resampled daily, respectively. Across-track velocities derived from the along-track product with a 10 days resolution (a, b, c) are shown in orange. (g) Location of the current-meter moorings, Jason track #26 and altimetric grid of the MGP.

Table 3
Root Mean Square Differences (rmsd, in cm s^{-1}) and Correlation Coefficients of Satellite-Altimeter-Derived Surface Velocities and Upper Current-Meter Velocities From 2014 to 2015, 2001 to 2003, and 1993 to 1995 Moorings

		In situ/gridded altimetry			
		2 days		20 days	
		Along	Across	Along	Across
2014–2015 current meter					
1A1 328 m	Rmsd	11.3	13.1	8.1	8.8
	R corcoef	0.5	0.8	0.7	0.9
	V corcoef	0.7		1.1	
1M2 377 m	Rmsd	11.8	14.3	7.8	9.5
	R corcoef	0.55	0.8	0.9	0.9
	V corcoef	0.9		1.5	
1M5 520 m	Rmsd	14.2	12.9	8.8	8.1
	R corcoef	0.65	0.68	0.85	0.82
	V corcoef	0.9		1.4	
2001–2003 current meter					
0M1 270 m	Rmsd	6.82	8.31	4.20	5.27
	R corcoef	0.47	0.71	0.72	0.86
	V corcoef	0.57		1.25	
0M4 215 m	Rmsd	6.89	8.12	5.53	7.02
	R corcoef	0.68	0.58	0.87	0.76
	V corcoef	0.79		1.23	
0M7 150 m	Rmsd	7.57	6.82	5.68	4.98
	R corcoef	0.57	0.84	0.71	0.91
	V corcoef	1.02		1.38	
1993–1995 current meter					
9M3 240 m	Rmsd	11.52	9.13	8.63	5.72
	R corcoef	0.71	0.74	0.76	0.87
	V corcoef	0.79		1.15	
9M6 340 m	Rmsd	8.62	7.91	7.3	5.39
	R corcoef	0.72	0.71	0.81	0.83
	V corcoef	1.13		1.47	
9M8 300 m	Rmsd	9.12	7.92	7.75	5.47
	R corcoef	0.77	0.72	0.85	0.84
	V corcoef	1.23		1.59	

Note. In situ data were 2–20 days low-pass-filtered with a resampling interval of 24 h. The surface velocities were computed from maps of absolute dynamic topography with a 1 day resolution from multisatellite gridded products. R corcoef is the correlation coefficient and V corcoef is the vector correlation coefficient squared following Crosby et al. (1993) between in situ and altimetry data. Correlations were significant at the 95% confidence level calculated according to the standard method (Emery & Thomson, 2001).

The ADT time series along the 2,000 m isobath (red isobath in Figure 4a) in the 38°S–42°S latitudinal band is shown in Figure 4c. The 2,000 m isobath was chosen because it falls close to the midpoint of the continental slope, it is rather straight (Figure 4a) and the MC and BC cores roughly lie above that depth. ADT values around −5 and 30 cm correspond to the location of maximum gradients in the record length mean ADT (not shown, similar procedure as in Barré et al. (2011)), and are associated with the position of the SAF and the Brazil Current Front (BCF), respectively. The variable position of the fronts as indicated by the ADT suggests migrations of the Brazil-Malvinas Confluence. In particular, during the last mooring period, the SAF remained at a southernmost position during 4 months. The SAF was in a northern position (∼39°S–40°S) during most of the 1990s and has shifted southward and remained around 39.5°S since 2000 (Figure 4c). In 2016, the position of the fronts is back north like in the 1990s. The mean position of the SAF during the most recent measurement period is the southernmost of the three observation periods. The mean SLA computed over each mooring period (full years were considered to avoid seasonal bias) is presented in Figure 5. For the last mooring deployment period, a large positive anomaly (up to 20 cm) is observed (well above the mean sea level rise effect which is less than 7 cm, e.g., Cazenave et al., 2014), which corresponds to a southward location of the SAF on the continental slope as well as a westward and southward displacement of

Table 4
Root Mean Square Differences (rmsd, in cm s^{-1}) and Correlation Coefficient (R corcoef) of Satellite-Altimeter-Derived Surface Velocities and Upper Current-Meter Velocities From 2014 to 2015, 2001 to 2003, and 1993 to 1995 Moorings

		Across-track component In situ/along-track altimetry	
		2 days	20 days
2013–2015 current meter			
1A1 328 m	Rmsd	15.23 (16%)	10.06 (14%)
	R corcoef	0.67 (0.13)	0.74 (0.16)
1M2 377 m	Rmsd	15.17 (6%)	11.81 (24%)
	R corcoef	0.71 (0.09)	0.83 (0.07)
1M5 520 m	Rmsd	13.69 (6%)	10.11 (20%)
	R corcoef	0.62 (0.06)	0.79 (0.03)
2001–2003 current meter			
0M1 270 m	Rmsd	10.41 (25%)	8.33 (58%)
	R corcoef	0.64 (0.07)	0.73 (0.13)
0M4 215 m	Rmsd	9.89 (22%)	8.24 (17%)
	R corcoef	0.48 (0.10)	0.61 (0.15)
0M7 150 m	Rmsd	9.53 (40%)	7.52 (51%)
	R corcoef	0.78 (0.06)	0.83 (0.08)
1993–1995 current meter			
9M3 240 m	Rmsd	12.98 (42%)	8.58(50%)
	R corcoef	0.61 (0.13)	0.69 (0.18)
9M6 215 m	Rmsd	11.76 (49%)	9.09 (68%)
	R corcoef	0.58 (0.13)	0.63 (0.20)
9M8 340 m	Rmsd	12.51 (58%)	7.81 (42%)
	R corcoef	0.57 (0.15)	0.59 (0.25)

Note. The surface velocities were computed using 10 day resolution along-track satellite data. Relative percentage differences in parentheses indicate the gain obtained in using multisatellite-gridded products compared to along-track products. Correlations were significant at the 95% confidence level.

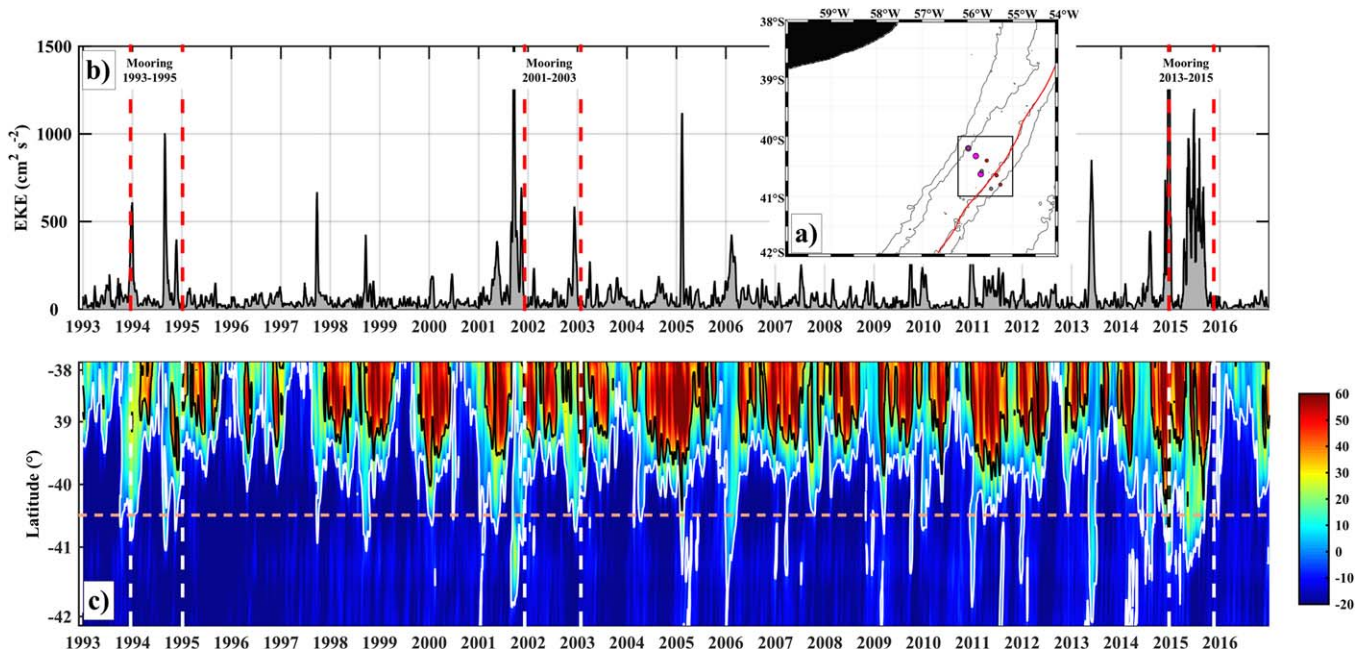

Figure 4. (a) Bottom topography and mooring locations. The 6,000, 5,000, 3,000, 1,000, and 300 m isobaths are represented with solid light grey contours, the 2,000 m contour is highlighted in red. (b) Surface Eddy Kinetic Energy estimated from MGP around mooring locations (black square in Figure 4a) over the period 1993–2016. (c) Absolute Dynamic Topography (ADT) along isobath 2000 m. The −5 and +30 cm ADT values corresponding to the SAF and BCF are marked with white and black lines, respectively. Mooring periods are indicated with vertical dashed lines. The dashed line at 40.5°S corresponds to the intersection of Jason track #26 and the 2,000 m isobath.

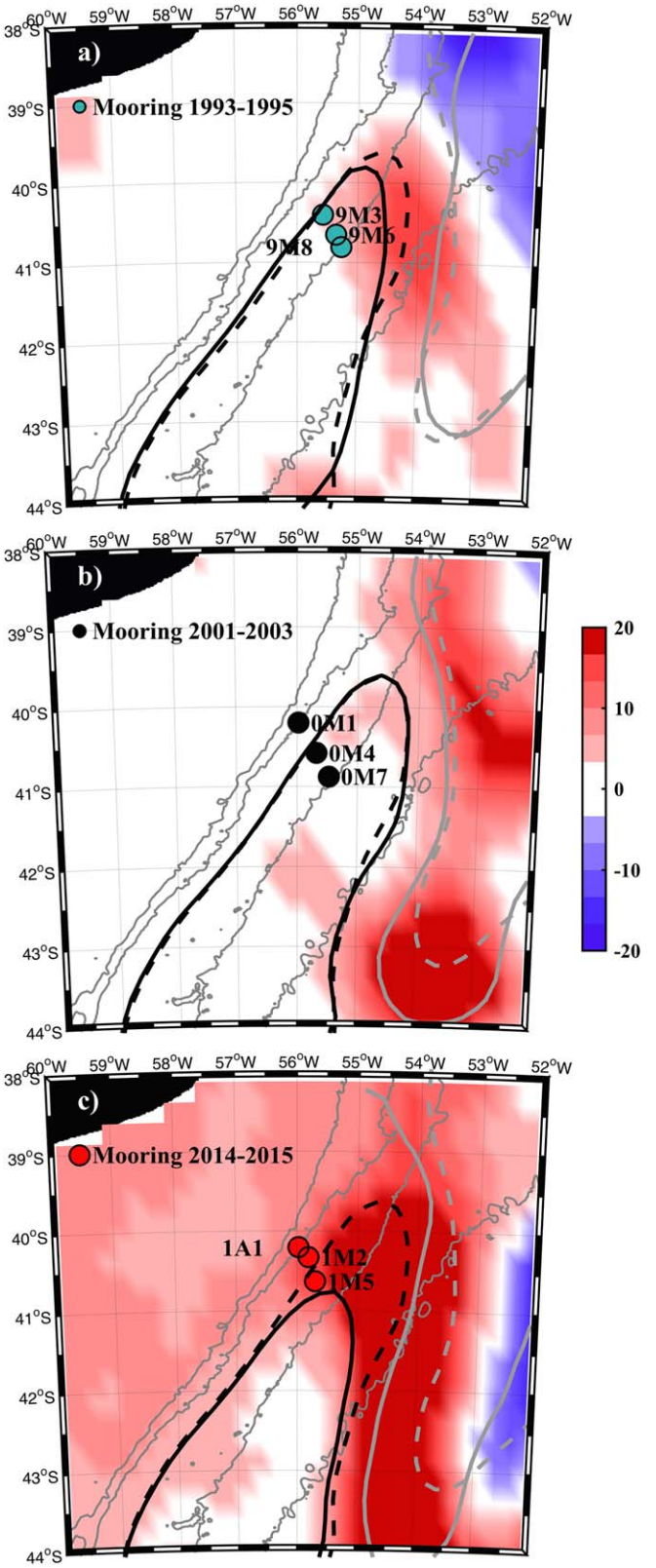

Figure 5. Mean of the Sea Level Anomalies (SLA) over the (a) 1993–1995, (b) 2001–2003, and (c) 2014–2015 measurement periods. Full years are considered to avoid seasonal biases. Black and grey solid (dashed) contours represented the SAF and BCF position during each period (whole altimetric period), respectively.

the BC overshoot. In contrast, the mean SLA over the mooring region during the other in situ observation periods does not exceed values larger than 8 cm. It is to be noted that the three measurement periods correspond to positive or small mean SLA at the mooring line.

4.2. Focus on the Singular 2014–2015 Period

Two regimes, "weak Malvinas" and "strong Malvinas," can be identified during the last mooring period. During the "strong Malvinas" regime (from early January to mid-April 2015 and from mid-August to the end of November 2015), the confluence is located north from the mooring array around 39°S and the MC surface velocities at the mooring location are large (~50 cm s^{-1}) (Figure 6a). During the "weak Malvinas" regime, that is during December 2014 and from May to September 2015, the MC retroflects close to the latitude of the mooring array, the surface velocities at inshore sites are smaller (~10 cm s^{-1}) and velocities at offshore locations rotated clockwise (Figure 6b). Stick plots of altimetry-derived surface geostrophic velocities (SGV) and in situ upper-level velocities (20 day low-pass) superimposed on the altimetry-derived EKE around the mooring array show the general agreement between SGV and in situ velocities and suggest a nontrivial relation between the magnitude of surface velocity and the regional EKE levels (Figure 7). Weak Malvinas periods are characterized by large EKE values, reaching peaks larger than 1,000 cm^2 s^{-2} while strong Malvinas periods are characterized by small EKE values lower than 200 cm^2 s^{-2} (Figure 7). Indeed variance ellipses are larger during weak Malvinas periods and it is also the case for altimetry-derived surface geostrophic velocities (not shown).

In the following, we examine the dominant modes of variations in the 20 day low-pass filtered in situ velocity and in the altimetry-derived surface geostrophic velocity. An empirical orthogonal function (EOF) analysis was carried out using the velocity data from three moorings all together from December 2014 to November 2015. We used 20 day low-pass-filtered in situ velocity time series at 1M2 (377, 823, and 1,106 m), 1M5 (520, 970, 1,264, and 1,663 m) and five levels from 1A1 (at 328, 424, 544, 808, and 976 m). The first EOF mode explains 70% of the total variance (Figures 8a and 8b) and its times series roughly represents the periods of weak and strong Malvinas Current with increased flow during strong Malvinas. At each mooring, the velocity vectors at different depths are almost parallel to each other except at 1M5 where an upward anticlockwise rotation is observed.

An EOF analysis was performed on the maps of sea level anomaly (MSLA) over the same time period and over the region of the Brazil/Malvinas Confluence centered on the mooring array. The first EOF of SLA explains 28% of the total variance and its spatial structure corresponds to a dipole with the mooring array being located on the southwestern edge of the negative part of the dipole (Figure 8a). The velocity anomaly vectors from EOF-1 SLA remarkably match the upper-level vectors of the mooring data EOF-1 (Figure 8a). The time series associated with the SLA EOF-1 is appreciably similar to the time series associated with the three moorings EOF-1 (Figures 8b and 8c), with a clear distinction between the two Malvinas Current regimes, weak and strong.

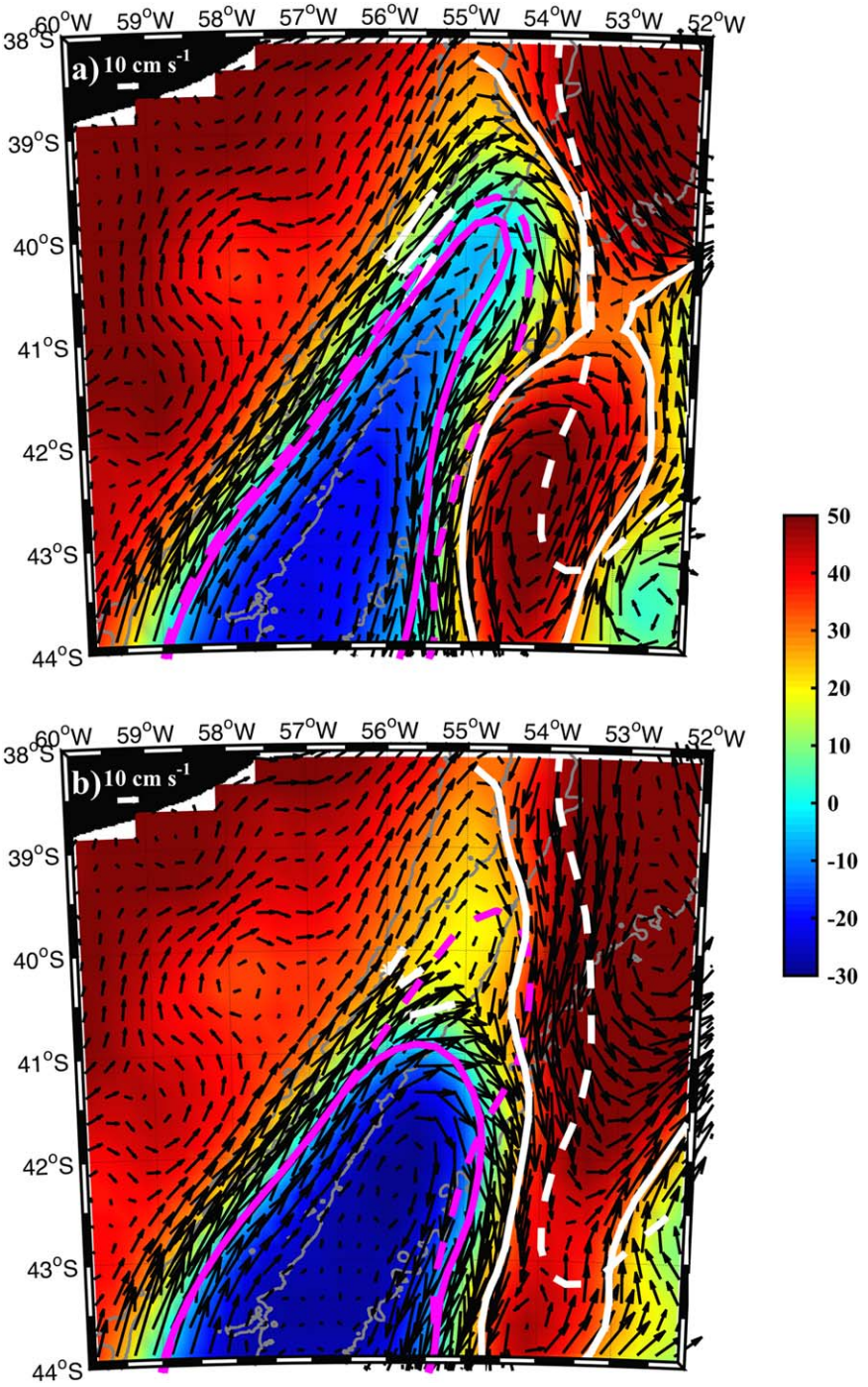

Figure 6. Absolute Dynamics Topography composites and mean surface geostrophic velocity fields for (a) the strong Malvinas Current regime and (b) the weak Malvinas Current regime. White arrows indicate mean in situ velocities of the upper current meters. The magenta and white solid (dashed) contours represent the SAF and BCF position during each period (whole altimetric period), respectively.

The negative phase of EOF-1 as shown in the ADT field obtained by subtracting EOF1 from the Mean Dynamic Topography (MDT − EOF-1) corresponds to a migration of the SAF over the mooring array (Figure 8d). A similar pattern is observed in the ADT fields corresponding to a minimum in the EOF-1 time series (example, from 1 August 2015, Figures 8c and 8f). At this time, the MC turns offshore and recirculates southward at about 40.5°S. In contrast, the ADT field associated with the positive phase (MDT + EOF-1) (Figure 8e) displays a

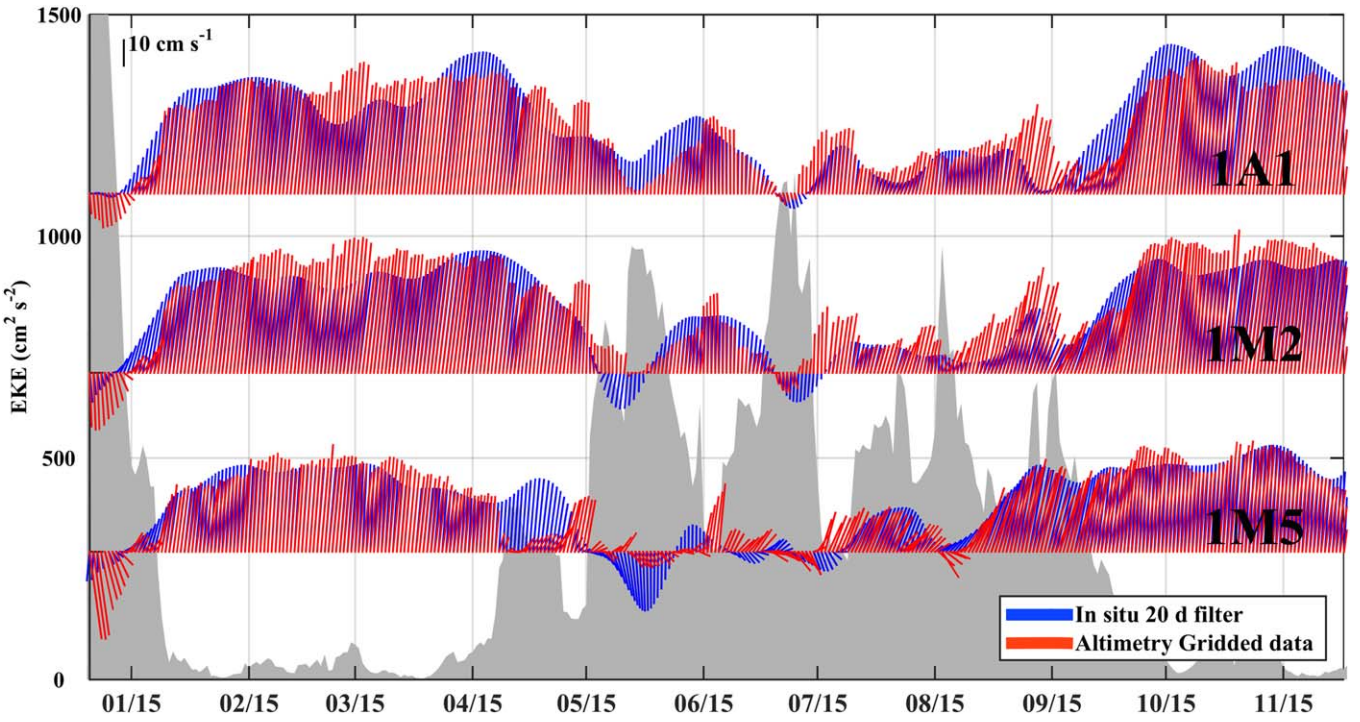

Figure 7. (a) Stick plots of the shallowest 20 day low-pass-filtered in situ velocity (in blue) and satellite-altimeter-derived surface velocity (in red) time series from 1A1, 1M2, and 1M5 superimposed to surface eddy kinetic energy estimated as Figure 4b over 2014–2015 mooring period.

circulation pattern similar to the one observed during the maximum of the time series of the EOF-1 in SLA reached on 26 October 2015 (Figures 8c and 8g) with a cyclonic meander located north east of the section extending the SAF and the Malvinas Current northward beyond the mooring array up to 38°S.

The agreement between the second EOF of SLA and in situ velocities (both explaining about 18% of their respective total variance) is not as straightforward (Figure 9). The SLA spatial structure of the EOF-2 shows a small eddy-like structure of roughly one degree in latitude and longitude at the location of the mooring and a larger and more intense dipole structure to the east (Figure 9a). The time series associated with SLA EOF-2 bears some similarity with the time series of the three moorings EOF-2 after mid-April (Figures 9b and 9c). The ADT map obtained adding the Mean Dynamic Topography to the negative phase of EOF-2 pattern corresponds to a northeastward deflection of the overshoot of the Brazil Current (Figure 9d). In contrast, the positive phase of EOF-2 corresponds to an overshoot of the Brazil Current flow extending south to 44°S almost parallel to isobaths (Figure 9e). The maps of absolute dynamic topography (MADT) from 16 May 2015 and 30 August 2015 (Figures 9f and 9g) reveal resembling spatial structures such as overshoot deflected to the east and overshoot parallel to the bathymetry, although differences are seen in the northward penetration of the MC which are represented by EOF-1. Several small eddy-like structures (diameter about 50 km) populate the region between the SAF and BCF (Figures 9f and 9g). The spatial resolution of altimetric data does not fully resolve these scales.

Overall EOF-1 can be associated with the northward penetration of the Malvinas Current and EOF-2 with an east-west deflection of the Brazil Current overshoot.

5. SLA Variations at the Brazil-Malvinas Confluence in the Altimetric Record

5.1. Modes of SLA Variations in the Brazil-Malvinas Confluence

An EOF decomposition of SLA variations was performed using the 24 years of detrended altimetric data to examine short-term fluctuations. The linear trend (Figure 10a) shows an SLA increase of about 15 cm in 24 years corresponding to a southern shift of the Brazil-Malvinas Confluence. The southern drift occurred at

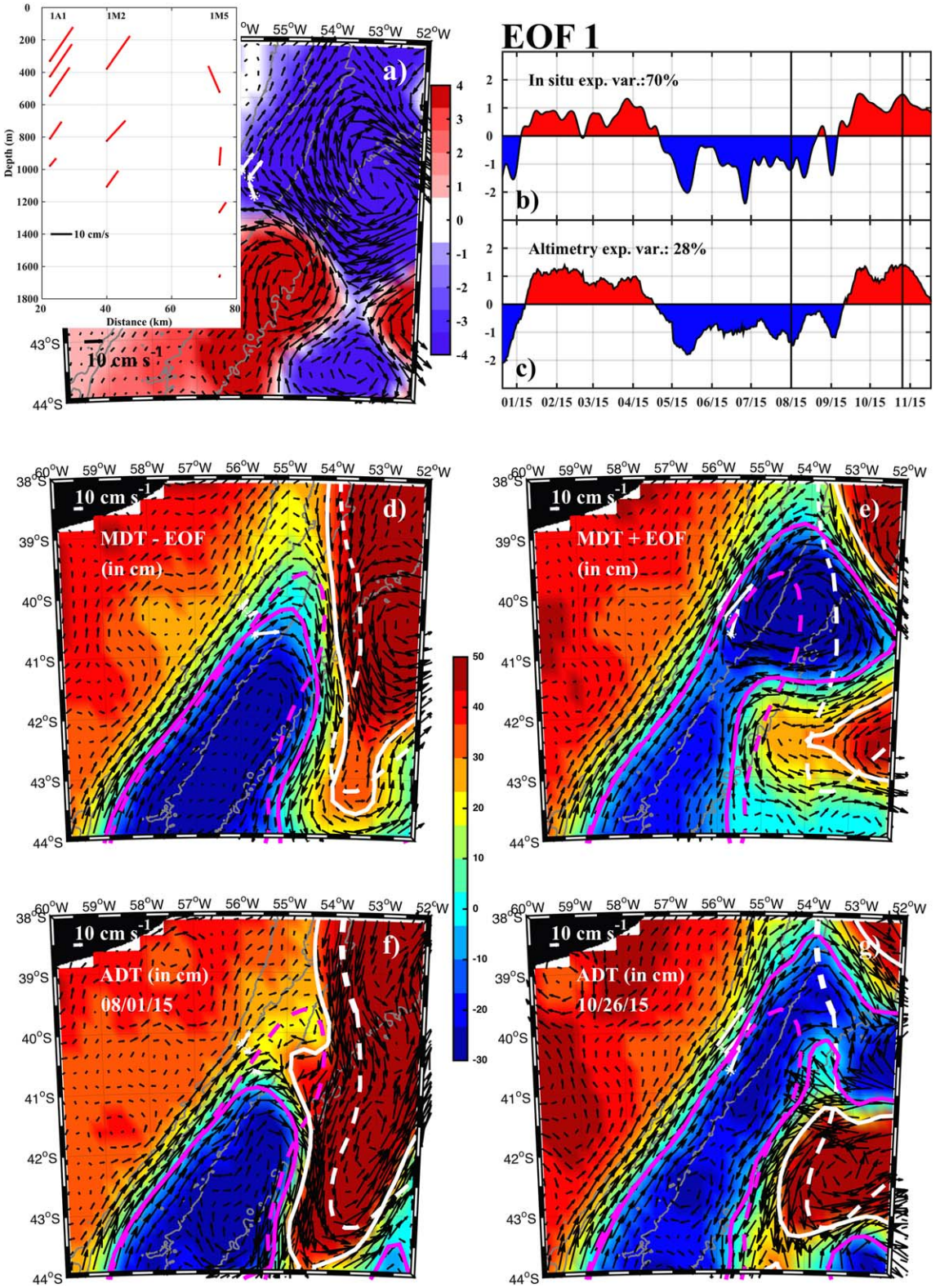

Figure 8. EOF analysis of the SLA and of the three moorings (1A1, 1M2, 1M5) taken together. (a) EOF-1 of SLA (black arrows: geostrophic velocities from the EOF-1 of SLA, white arrows upper level of in situ velocity EOF-1). Upper left plot, vectors of EOF-1 of the three moorings taken together in red. (b) Time series associated with EOF-1 of the three moorings. (c) Time series associated with EOF-1 of SLA. (d) Absolute dynamic topography (ADT) corresponding to the negative phase of EOF-1: MDT − EOF-1. (e) ADT corresponding to the positive phase of EOF-1: MDT + EOF-1. (f) ADT on 1 August 2015, (g) ADT on 26 October 2015. Magenta and white solid (dashed) contours represent the SAF and BCF position for the corresponding dates (mean over 1993–2016).

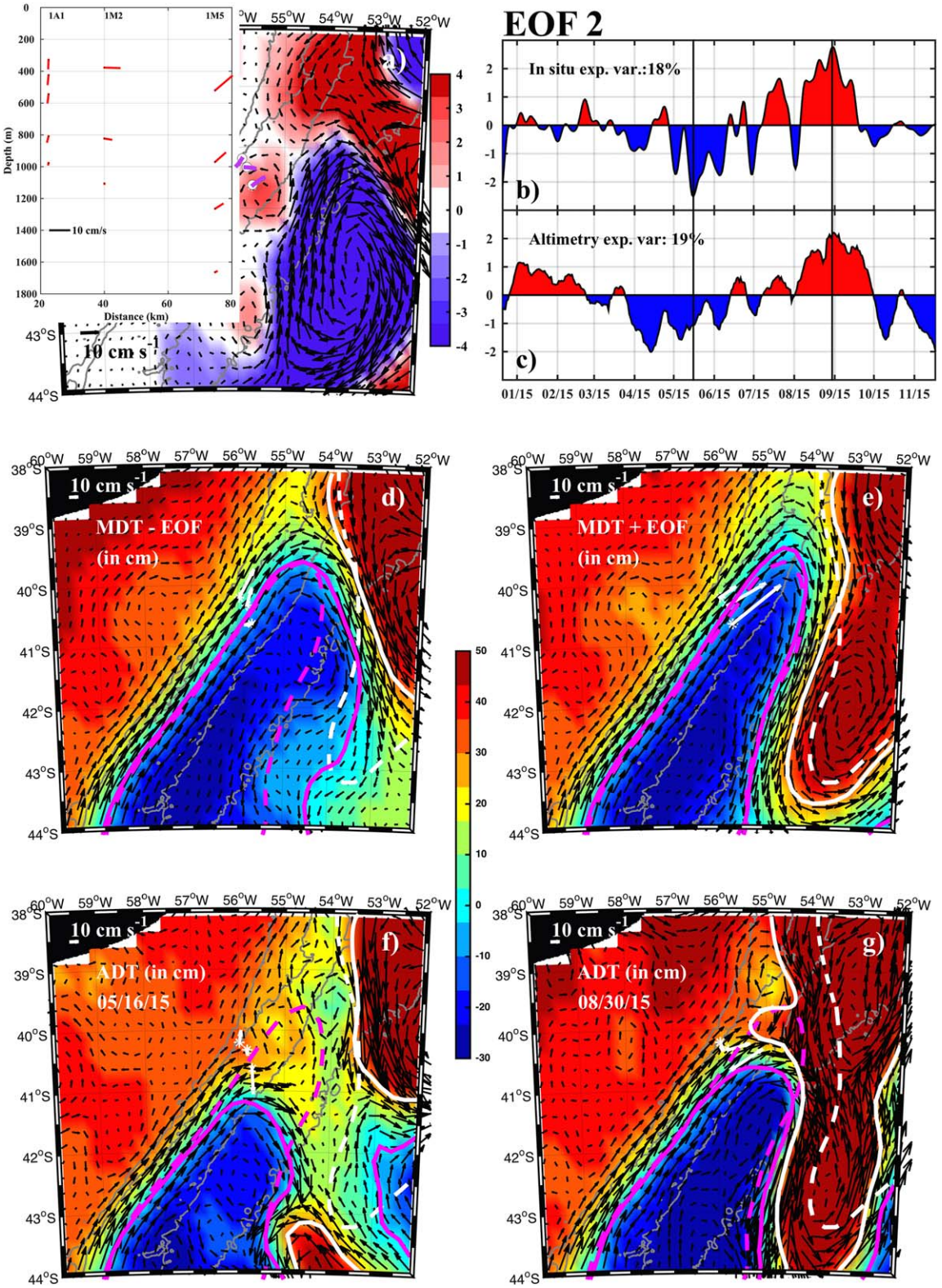

Figure 9. EOF analysis of the SLA and of the three moorings taken together. (a) EOF-2 of SLA (black arrows: geostrophic velocities from the EOF-2 of SLA, magenta arrows upper level of in situ velocity EOF-2). In the upper left plot, vectors of EOF-2 of the three moorings taken together are indicated in red. (b) Time series associated with EOF-2 of the three moorings. (c) Time series associated with EOF-2 of SLA. (d) Absolute dynamic topography (ADT) corresponding to the negative phase of EOF-2: MDT − EOF-2. (e) ADT corresponding to the positive phase of EOF-2: MDT + EOF-2 (f) ADT on 16 May 2015. (g) ADT on 30 August 2015. Magenta and white solid (dashed) contours represent the SAF and BCF position for the corresponding dates (mean over whole altimetric period).

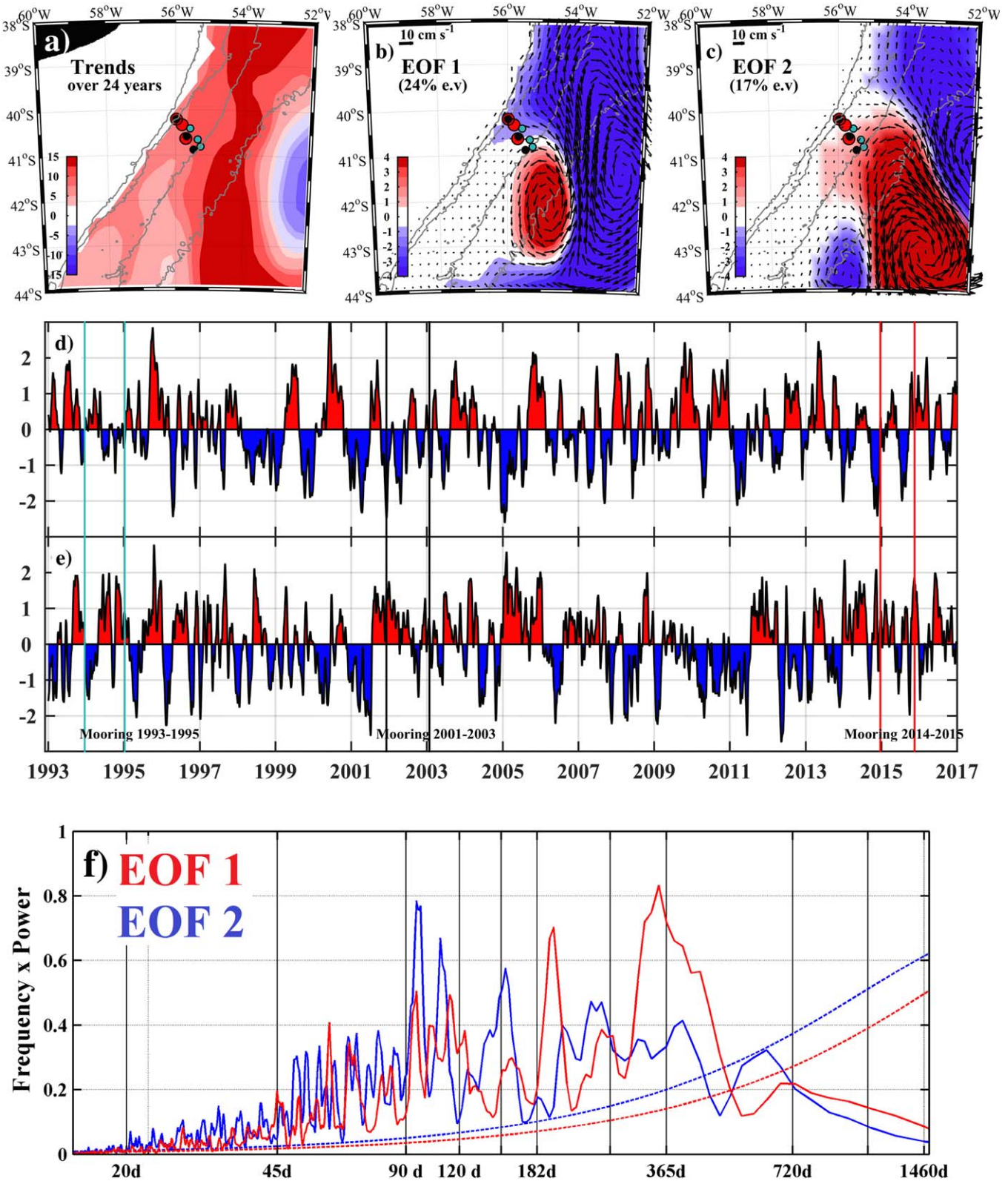

Figure 10. (a) Linear trend in SLA (in cm) over 1993–2016 (b) EOF-1 and (c) EOF-2 of the SLA over 1993–2016. Time series associated with (d) EOF-1 and (e) EOF-2. (f) Spectrum of the EOF time series (EOF-1 in red, EOF-2 in blue). Dashed lines indicate the confidence limit interval at 95%.

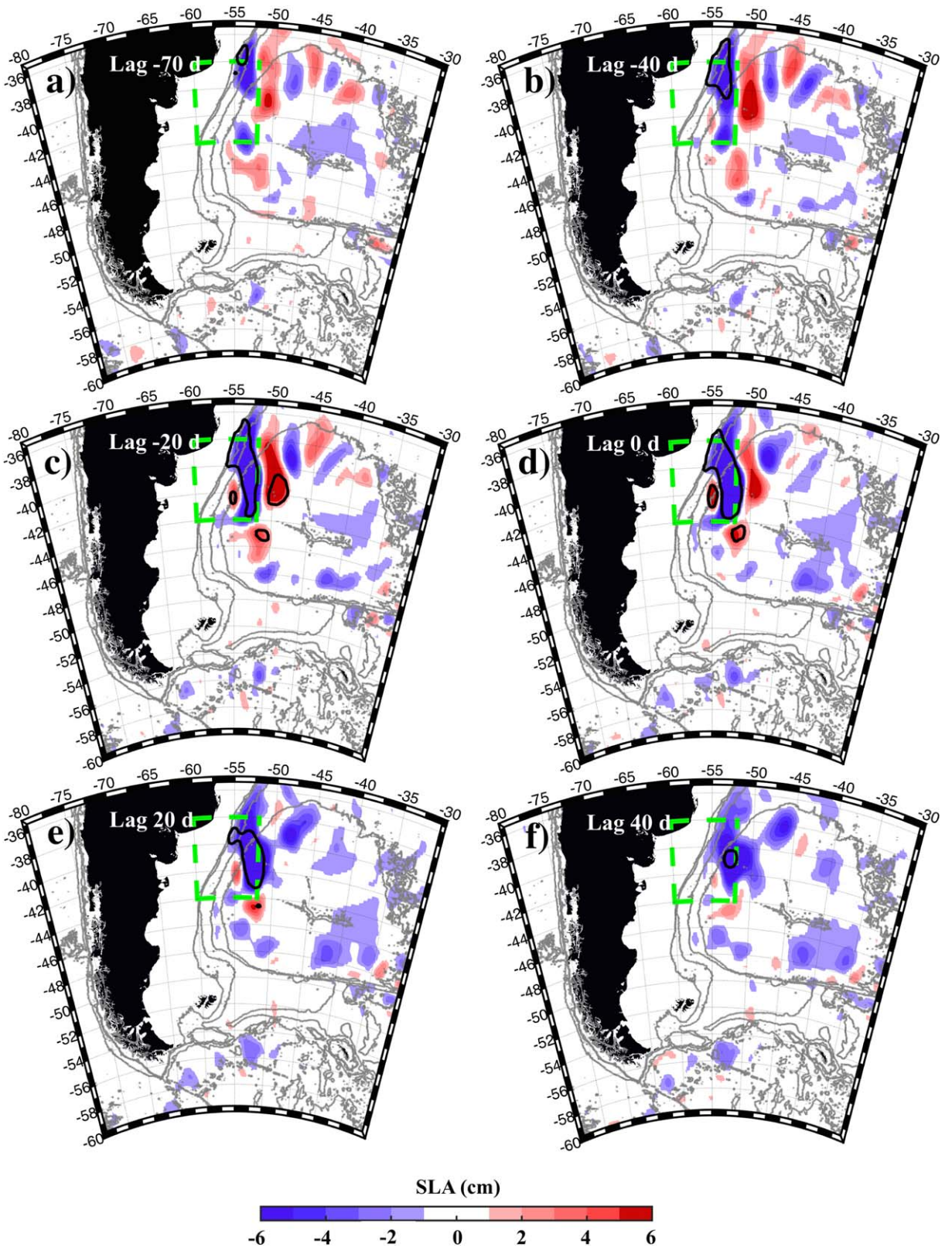

Figure 11. Regression of SLA on the normalized time series associated with EOF-1 at different lags. Black solid contour represents the correlation at 90% confidence level. Isobaths are the same as in Figure 1.

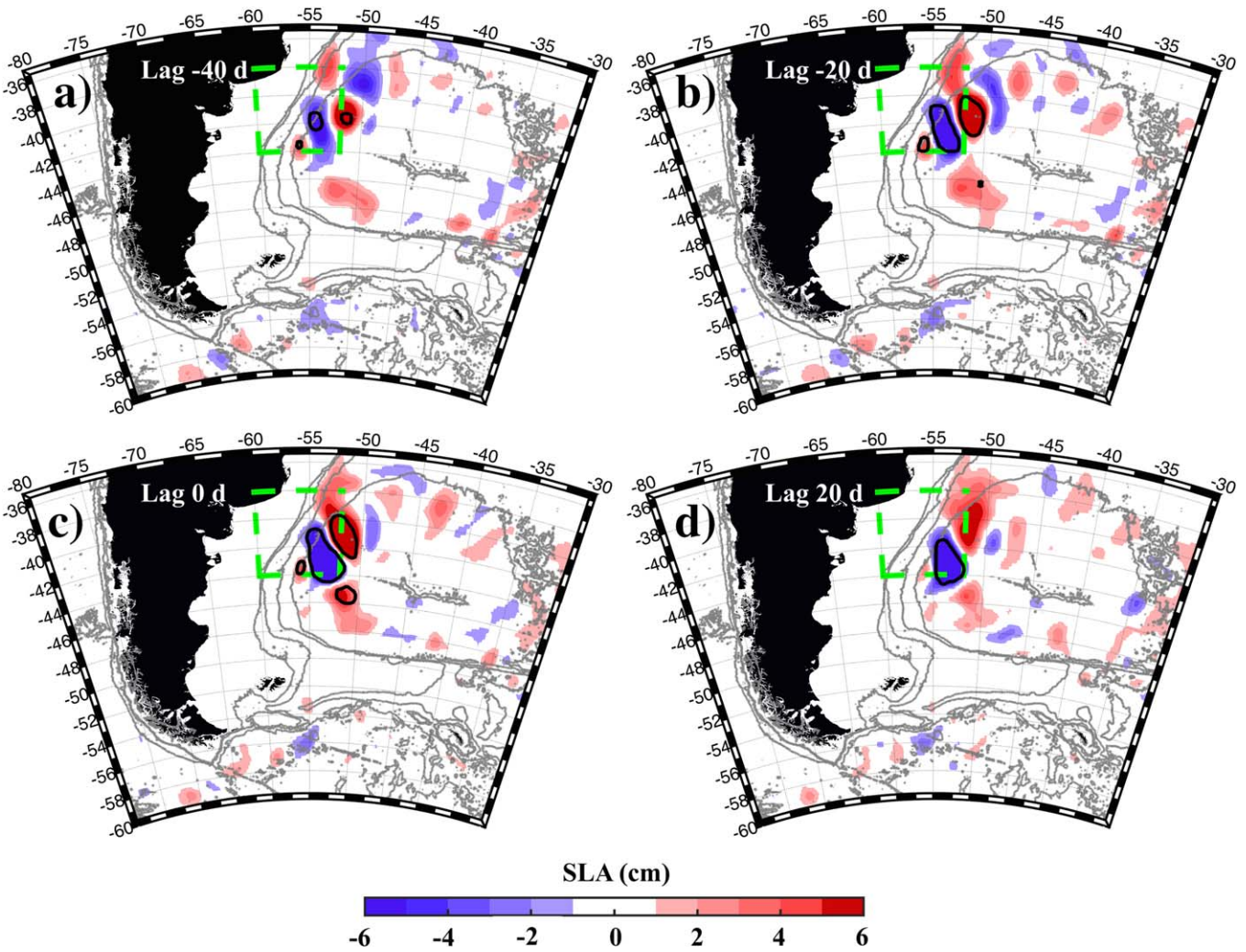

Figure 12. Regression of SLA on the normalized time series associated with EOF-2 at different lags. Black solid contour represents the correlation at 90% confidence level. Isobaths are the same as in Figure 1.

the end of the 1990s beginning of the 2000s, the northern penetration of the MC remained at a southern location from year 2002 to 2015 and, in 2016 returned to a location back north as in 1993 (Figure 4c).

The first two EOFs bear some resemblance to the ones obtained over the 2014–2015 period (Figures 10b and 10c) and explained a similar amount of the total variance (24% EOF-1 and 17% EOF-2). These first two EOF modes are robust dominant modes with large amplitudes (maxima $>$ 40 cm). They show up as the first two modes in the EOF decompositions we produced over the periods of the first two current-meter arrays and always explained more than 20% of the variance (not shown). As in section 4.2, EOF-1 is a dipole associated with the latitudinal migrations of the Brazil-Malvinas Confluence and EOF-2 is a dipole associated with longitudinal excursions of the overshoot of the Brazil Current. The associated time series (Figures 10d and 10e) are similar to those in Figures 8c and 9c for the corresponding time range (December 2014 to November 2015).

The spectral content of EOF1 time series features dominant energy peaks around the annual and semiannual periods and a significant (at 95% CL) energy content in a broad band from 45 to 140 days (Figure 10f, in red). The spectrum of EOF-2 time series shows more energy at higher frequencies and, in particular, features three high-energy peaks at periods between 3 and 5 months, well above the level of energy at the semiannual and annual periods (Figure 10f, in blue). The two modes show some energy at lower frequencies, with a 1.5 year period for EOF2 and 2 year period for EOF-1 (both significant at 90% CL, not shown).

These results suggest that latitudinal migrations of the Brazil-Malvinas Confluence have a dominant semiannual/annual variability while the longitudinal excursions of the overshoot of the BC vary at higher frequencies.

5.2. Regression of the Southwest Atlantic SLA on the Confluence Modes

In an attempt to put the SLA modes of variation in the Brazil-Malvinas Confluence in a larger spatial context, the SLA field in the Southwest Atlantic was regressed on the time series of the first two EOF shown in Figure 10. Selected lagged regression maps show quite similar structures, with significant regressions (above the 90% confidence level) being observed in an area extending from 36°S to 45°S and 58°W to 47°W and over a 100 day range of lags (Figures 11 and 12).

The zero lag regression maps correspond to the EOF patterns (Figure 10) and provide information on the scales of the structures that extend beyond the region where the EOFs were calculated (Figures 11 and 12). The large negative pattern of EOF-1 impinging on the slope has a meridional extension of 8 degrees. The time scale associated with this regression is annual and the regression maps at lag −180 and +180 days show a positive anomaly on the slope between 40°S and 37°S (not shown). Regression maps at lag 0 for EOF-1 and EOF-2 present differences: the significant SLA patterns in the regression map for EOF-1 are located on or close to the continental slope whereas significant SLA patterns in the regression map for EOF-2 are found offshore. This is consistent with EOF-1 representing latitudinal motions along the slope and EOF-2 longitudinal variations in the offshore location of the overshoot. In contrast to EOF-1, the time scale associated with the regression onto EOF-2 cannot be clearly estimated from a change in sign in the regression pattern: this is consistent with the fact that no single energy peak dominates the spectrum of the second mode (Figure 10e).

Regression maps onto time series associated with the EOF-1 (Figure 11) suggest a pattern of standing organized wave train like of mesoscale SLA along the northern side of the Argentine Basin from lag −70 days with a growing amplitude up to lag −10 days. A westward propagation of anomalies against the mean flow could cause this remarkable standing pattern. The pattern vanishes at lag 0. Regression patterns with EOF-2 (Figure 12) have significant regressions only from lag −40 to +20 days and also show an organized standing wave train on the northern side of the Argentine Basin from lag −40 days to 0. In both lagged regression map series (EOF-1 and EOF-2), propagations of anomalies are difficult to identify and regression patterns do not give much clue about the processes responsible for their existence.

6. Summary and Conclusions

Altimetry-derived surface velocities were compared to year long current-meter velocities obtained from moorings deployed in the 1990s, 2000s, and in 2015 at 41°S in the Malvinas Current near its confluence with the Brazil Current. This comparison is a stringent test as spatial and temporal scales in the Confluence can be small relative to the scales that are resolved by satellite altimetry (Barré et al., 2006; Pujol et al., 2016). It was found that the multisatellite gridded products (MGP) are highly correlated ($>$0.8) with the 20 day low-pass filtered velocity from the upper current meters (at about 300 m depth) with an rmsd of 7 cm/s. Correlations are larger for along-isobaths velocities (0.85) than for cross isobaths velocities (0.8). The MGP provide better results than the along-track products. The satisfactory comparison between altimetry products and the in situ velocities led us to combine the MGP and in situ data to compute a 24 year long volume transport time series of the MC at 41°S. The MGP were used here to put the three in situ measurement periods in a wider regional and temporal perspective.

The most recent measurement period (2014–2015) is characterized by a long-lasting high level of eddy kinetic energy (EKE) that is found to be concurrent with a southern location of the SAF. From 1993 until the end of 2016, year 2015 stands out as the year with the largest annual mean EKE at 41°S and the southernmost mean location for the SAF (Figure 4). The last in situ measurement period (2014–2015) comprises two distinct regimes referred to as "weak Malvinas" and "strong Malvinas." The altimetry data showed that the "weak Malvinas" regime corresponds to a southern position of the SAF on the mooring line (and high local EKE) and the "strong Malvinas" regime to a northern SAF location (and low local EKE). The first two modes of variations of SLA over an area of 6° in latitude × 8° in longitude centered at the mooring array were found in excellent agreement with the modes of variations of the low-passed in situ velocities. The first SLA

mode displays a dipole associated with the meridional migrations of the penetration of the Malvinas Current, and the second mode with a zonal displacement of the Brazil Current overshoot.

These two modes are robust and stand out in an EOF analysis of the 24 year long time series of SLA over the Brazil-Malvinas Confluence region. Over the 24 years, the latitudinal migrations of the penetration of the Malvinas Current (the first mode explaining 24% of the total variance) are dominated by semiannual and annual variations whereas the longitudinal excursions of the Brazil Current overshoot (second mode explaining 17% of the total variance) feature larger energy peaks at shorter periods of a few months (3, 4, and 5 months). The semiannual and annual variations observed in the northward penetration of the Malvinas Current are reminiscent of the prealtimetric observations from Garzoli and Garraffo (1989) and correspond to the semiannual and annual variations found in the Malvinas Current transport near the Confluence (e.g., Spadone & Provost, 2009; Vivier et al., 2001).

The SLA from the southwest Atlantic (50° in longitude × 25° in latitude) were regressed onto the time series of the two EOF modes computed over the BMC showing the rather large scales of the pattern and remarkable standing wave train like structures in the Argentine Basin. The dynamical mechanisms responsible for the first two modes have yet to be investigated. Statistical relationships with local wind stress and wind stress curl were investigated and did not lead to any concluding results.

We focused on variations at time scales less than 2 years. Long-term variations are beyond the scope of this work as the record length of satellite altimetry data is still too short to study variations at low frequencies from SLA alone in this complex region. The low frequency variations of the location of the Brazil-Malvinas Confluence have been examined from observational, theoretical, or modeling points of view (e.g., Combes & Matano, 2014; Goni et al., 2011; Lebedev & Nof, 1996; Lumpkin & Garzoli, 2011) without a definitive conclusion and the subject remains open. Outputs from operational model reanalyses may help in this regard.

Acknowledgments
The authors are deeply grateful to the Centre National d'Etudes Spatiales (CNES) for the constant support. This study is a contribution to EUMETSAT/CNES DSP/OT/12–2118 and CONICET-FYPF PIO 133–20130100242. We acknowledge support from the MINCYT-ECOS-Sud A14U0 projects ECOS-Sud program in facilitating scientific exchanges between Argentina and France. Camila Artana is funded under a PhD scholarship from Université Pierre et Marie Curie. The satellite data are available at Copernicus Marine Environment monitoring service (CMEMS) (http://marine.copernicus.eu/) and the in situ data are available at SEANOE (www.seanoe.org, cf., references below Provost et al., 2017a, 2017b; Saraceno et al., 2017).

References

Artana, C., Ferrari, R., Koenig, Z., Saraceno, M., Piola, A. R., & Provost, C. (2016). Malvinas Current variability from Argo floats and satellite altimetry. *Journal of Geophysical Research: Oceans*, *121*, 4854–4872. https://doi.org/10.1002/2016JC011889

Barré, N., Provost, C., Renault, A., & Sennéchael, N. (2011). Fronts, meanders and eddies in Drake Passage during the ANT-XXIII/3 cruise in January-February 2006: A satellite perspective. *Deep Sea Research, Part II*, *58*, 2533–2554. https://doi.org/10.1016/j.dsr2.2011.01.003

Barré, N., Provost, C., & Saraceno, M. (2006). Spatial and temporal scales of the Brazil-Malvinas Current confluence documented by simultaneous MODIS Aqua 1.1-km resolution SST and color images. *Advances in Space Research*, *37*, 770–786. https://doi.org/10.1016/j.asr.2005.09.026

Cazenave, A., Dieng, H. B., Meyssignac, B., von Schuckmann, K., Decharme, B., & Berthier, E. (2014). The rate of sea level rise. *Nature Climate Change*, *4*, 358–361. https://doi.org/10.1038/nclimate2159

Chelton, D. B., Schlax, M. G., Samelson, R. M., & de Szoeke, R. A. (2007). Global observations of large oceanic eddies. *Geophysical Research Letters*, *34*, L15606. https://doi.org/10.1029/2007GL030812

Combes, V., & Matano, R. (2014). Trends in the Brazil/Malvinas Confluence region. *Geophysical Research Letters*, *41*, 8971–9877. https://doi.org/10.1002/2014GL062523

Crosby, D. S., Breaker, L. C. & Gemmill, W. H. (1993). A proposed definition for vector correlation in geophysics: Theory and application. *Journal of Atmospheric and Oceanic Technology*, 10, 355–367. https://doi.org/10.1175/1520-0426(1993)010<0355:APDFVC>2.0.CO;2

Emery, W. J., & Thomson, R. E. (2001). *Data analysis methods in physical oceanography* (2nd ed.). Amsterdam, the Netherlands: Elsevier.

Fu, L.-L. (2006). Pathways of eddies in the South Atlantic Ocean revealed from satellite altimeter observations. *Geophysical Research Letters*, *33*, L14610. https://doi.org/10.1029/2006GL026245

Fu, L.-L. (2007). Interaction of mesoscale variability with large-scale waves in the Argentine Basin. *Journal of Physical Oceanography*, *37*, 787–793. https://doi.org/10.1175/JPO2991.1

Fu, L.-L., Cheng, B., & Qiu, B. (2001). 25-day period large-scale oscillations in the Argentine Basin revealed by the TOPEX-Poseidon altimeter. *Journal of Physical Oceanography*, *31*, 506–517.

Garzoli, S. L., & Garraffo, Z. (1989). Transports, frontal motions and eddies at the Brazil-Malvinas Currents Confluence. *Deep Sea Research, Part A*, *36*(5), 681–703.

Goni, G. J., Bringas, F., & DiNezio, P. N. (2011). Observed low frequency variability of the Brazil Current front. *Journal of Geophysical Research*, *116*, C10037. https://doi.org/10.1029/2011JC007198

Lebedev, I., & Nof, D. (1996). The drifting Confluence Zone. *Journal of Physical Oceanography*, *26*, 2429–2448.

Lumpkin, R., & Garzoli, S. (2011). Interannual to decadal changes in the western South Atlantic's surface circulation. *Journal of Geophysical Research*, *116*, C01014. https://doi.org/10.1029/2010JC006285

Mason, E., Pascual, A., Gaube, P., Ruiz, S., Pelegri, J. L., & Delepouille, A. (2017). Subregional characterization of mesoscale eddies across the Brazil Malvinas Confluence. *Journal of Geophysical Research*, *122*, 3329–3357. https://doi.org/10.1002/2016JC012611

Peterson, R. G., & Stramma, L. (1991). Upper-level circulation in the South Atlantic Ocean. *Progress in Oceanography*, *26*(1), 1–73. https://doi.org/10.1016/0079-6611(91)90006-8

Piola, A. R., Franco, B. C., Palma, E. D., & Saraceno, M. (2013). Multiple jets in the Malvinas Current. *Journal of Geophysical Research: Oceans*, *118*, 2107–2117. https://doi.org/10.1002/jgrc.20170

Provost, C., Lanoiselle, J., Kartavtseff, A., Vivier, F., Artana, C., & Durand, I. (2017a). *Malvinas Current 1993–1995: Mooring velocities*. SEANOE. Retrieved from www.seanoe.org; https://doi.org/10.17882/51483

Provost, C., Lanoisellé, J., Kartavtseff, A., Spadone, A., Artana, C., & Durand, I. (2017b). *Malvinas Current 2001–2003: Mooring velocities*. SEANOE. Retrieved from www.seanoe.org; https://doi.org/10.17882/51479

Provost, C., & Le Traon, P.-Y. (1993). Spatial and temporal scales in altimetric variability in the Brazil-Malvinas Current confluence region: Dominance of the semi-annual period and large spatial scales. *Journal of Geophysical Research*, *98*, 18037–18051.

Pujol, M.-I., Faugère, Y., Taburet, G., Dupuy, S., Pelloquin, C., Ablain, M., & Picot, N. (2016). DUACS DT2014: The new multi-mission altimeter data set reprocessed over 20 years. *Ocean Science*, *12*, 1067–1090. https://doi.org/10.5194/os-12-1067-2016

Saraceno, M., Guerrero, R., Piola, A. R., Provost, C., Perault, F., Ferrari, R.,. . . Artana, C. (2017). *Malvinas Current 2014–2015: Mooring velocities*. SEANOE. https://doi.org/10.17882/51492

Saraceno, M., & Provost, C. (2012). On eddy polarity distribution in the southwestern Atlantic. *Deep Sea Research, Part I*, *69*, 62–69. https://doi.org/10.1016/j.dsr.2012.07.005

Saraceno, M., Provost, C., & Zajaczkovski, U. (2009). Long-term variation in the anticyclonic ocean circulation over the Zapiola Rise as observed by satellite altimetry: Evidence of possible collapses. *Deep Sea Research, Part I*, *56*, 1077–1092. https://doi.org/10.1016/j.dsr.2009.03.0005

Smith, W. H. F., & Sandwell, D. T. (1994). Bathymetric prediction from dense satellite altimetry and sparse shipboard bathymetry. *Journal of Geophysical Research*, *99*, 21803–21824.

Spadone, A., & Provost, C. (2009). Variations in the Malvinas Current volume transport since October 1992. *Journal of Geophysical Research*, *114*, C02002. https://doi.org/10.1029/2008JC004882

Vivier, F., & Provost, C. (1999a). Direct velocity measurements in the Malvinas Current. *Journal of Geophysical Research*, *104*, 21083–21103.

Vivier, F., & Provost, C. (1999b). Volume transport of the Malvinas Current: Can the flow be monitored by TOPEX/Poseidon? *Journal of Geophysical Research*, *104*, 21105–21122.

Vivier, F., Provost, C., & Meredith, M. (2001). Remote and local forcing in the Brazil Malvinas Region. *Journal of Physical Oceanography*, *31*, 892–913. https://doi.org/10.1175/1520-048510.1175/1520-0485(2001)031 < 0892:RALFIT>2.0.CO;2